Flexible and bendable acoustofluidics based on ZnO film coated aluminium foil

Yong Liu,[a,b] Yifan Li,[b] Ahmed. M. el-Hady,[c] C. Zhao,[b] J. F. Du,[a] Yang Liu,[a,*] Y. Q. Fu [b,*]

[a]*State Key Laboratory of Electronic Thin Films and Integrated Devices, University of Electronic Science and Technology of China, Chengdu 610054, People's Republic of China*

[b]*Faculty of Engineering and Environment, University of Northumbria, Newcastle upon Tyne, NE1 8ST, UK*

[c] *Institute of Thin Film Sensing and Imaging, University of the West of Scotland, Paisley, UK, PA1 2BE*

ZnO coated Al foil of 50 μm thick was used to fabricate flexible and bendable acoustofluidic devices with various wavelengths (from 64 to 800 μm). Different acoustic wave modes (including Lamb waves and Rayleigh waves) were obtained experimentally and verified from theoretical analysis. Flexibility and deformability of the ZnO/Al foil acoustic wave devices were demonstrated by (1) deformation testing by bending the acoustic wave devices with strain values up to 1.375%; (2) fatigue testing by bending the devices for two thousand cycles. Using Lamb waves and Rayleigh waves generated from the ZnO/Al foil acoustofluidic devices, functions of droplet streaming and pumping were demonstrated using the flexible acoustic wave devices under different bending and twisting positions.

1. Introduction

* Corresponding authors, Prof. Yang Liu, E-mail: yliu1975@uestc.edu.cn; Dr. Richard Fu, E-mail: Richard.Fu@northumbria.ac.uk

Flexible and bendable electronics and micro-electromechanical system (MEMS) devices have recently been received significant attention for a wide range of applications such as compact electronics packaging (e.g. smartphone internal components), flexible displays, surgical treatment, wearable medical sensing, drug delivery, micro-total analysis system (μTAS) and wearable consumer devices [1-7]. They have demonstrated superior advantages over rigid solutions for flexibility, deformability, space reduction, integration and operation within complex shapes and structures. Flexible ultrasonic or acoustic wave sensors/actuators have been proposed for non-destructive ultrasonic testing [8-10], energy harvesting [11, 12], and sensing in liquids [13]. Acoustic wave (AW) technologies, especially thin film surface acoustic wave (SAW) devices, have been investigated extensively for integrated lab-on-chip and μTAS applications [14-21]. ZnO thin film based SAW microfluidic devices fabricated on the flexible polymer substrates have also been demonstrated [22- 24]. However, there are significant challenges with realizing efficient acoustic microfluidic functions on these polymer substrates, including significant attenuation and dissipation of acoustic wave and energies into polymer, poor film crystallinity and poor adhesion of thin film on the polymer substrates.

This paper, for the first time, theoretically analysed and experimentally demonstrated the efficient and high performance flexible and deformable acoustofluidics based on ZnO films (5 μm) deposited onto commercially available aluminium foil (50 μm). The Al foil substrate promotes texture growth of ZnO film, provides good film adhesion, and reduces film stress during film deposition, all of which are superior compared to those on a polymer substrate. Al foils, compared with their polymer counterparts, have distinct advantages of deformability (forming and then maintaining temporary shapes) and re-deformability (easily returning back to their un-deformed shape), and they thus solve many common problems associated with most of polymer based flexible devices (for example, large energy dissipation and permanent deformed

shapes). Using commercially available large area Al foils and thin film process, mass-production or roll-to-roll processes with a low-cost could be realized to fabricate high performance flexible/deformable acoustic wave sensors and microfluidic devices. However, there is not any report on flexible acoustofluidics using Al foils as substrates, although Al foil has been used as flexible electrodes on rigid $LiNbO_3$ based SAW substrates [24].

2. Experimental

ZnO films (5 μm thick) were sputtering deposited onto commercial aluminium foil (with thicknesses of 50 ± 5 μm in rectangular shapes with dimensions of 250 mm × 150 mm) using a Zn target (300×100 mm^2) at a DC power of 500 W, an Ar/O_2 flow ratio of 50/50 SCCM (Standard Cubic Centimetre per Minute) without any intentional substrate heating. During the deposition, the substrate holder was rotated to improve uniformity. The substrate to target distance was 20 mm and gas pressure was 5 mTorr.

The Al foils coated with ZnO films were attached onto a silicon carrier wafer, and the SAW delay lines were fabricated by patterning Cr/Au interdigital transducers (IDTs) using a conventional lift-off process. The IDTs were designed with a spatial periodicity or wavelengths of 64 μm to 800 μm, with 30 pairs of fingers and an aperture of 4.9 mm. The distance between the centres of a pair of IDTs was 10 mm. The frequency response spectra of the SAW devices were measured using a vector network analyzer (Agilent E5061B).

Flexibility, deformability and re-deformability of the Al foil based devices were demonstrated by substrate bending characterizations. The device (with a wavelength of 64 μm) was bent to different angles with different strains and the transmission signals were continuously measured

using the network analyser. Fatigue and cycling performance of the device were evaluated by bending the device with a fixed strain 0.6% for up to 2000 cycles, and the surface morphology and transmission characteristics were continuously monitored during bending. The bending was created by a mechanical bending vise where steel tubes with different diameters were put under the Al foil at the bending center. The device was then taken out and straightened again.

For effective microfluidic droplet manipulation, the surfaces of the devices were coated with a 200 nm thick hydrophobic layer of CYTOP^{TM} (Asahi Glass Co. Ltd.). The devices were mounted onto a bulk aluminium alloy test-holder in order to minimize the possible heating effects. For SAW generation, the devices were actuated using an RF signal generator (Agilent Technologies, N9310A), which was amplified using a broadband power amplifier (Amplifier Research, 75A250). The signal generator and the amplifier both had 50 Ω output resistance, and we used 50 Ω wires to connect the signal generator, the amplifier and the device to minimize internal reflection of the RF signals. Thus the system had less signal loss during the signal transmission path. The de-ionized (DI) droplets of 2.5 μL were placed onto the flexible devices, 2 mm in front of the SAW IDTs. The microfluidic behaviour of de-ionized water droplets were recorded using a high speed video camera (Vision Research, phantom V7.3) working at a frame rate of 4000 frames/s. Droplet pumping speeds were estimated based on the recorded videos and the frame rates.

3. Results and discussions

3.1. Frequency and vibration mode characterisation

Fig. 1 shows the measured frequency (S11) spectra of the devices with two types of wavelengths, and different peak positions corresponding to different wave modes have been marked. The

Lamb waves (including A_0 and S_0 modes) can be clearly identified for most of devices which matches the theoretical values calculated based on the substrate thickness. The measured results of frequency values for different devices with different wave modes are summarised in Fig. 2.

If thicknesses of the ZnO film and Al foil are fixed, with the increment of wavelength (λ) of acoustic waves, the wave modes will change from a pure Rayleigh type wave (when the wavelength is significantly smaller than the thickness of the device) into a mixture of Lamb and Rayleigh waves and then finally into pure Lamb waves (when the wavelength is much larger than the thickness of the devices). The frequencies for the Lamb wave A_0 mode and S_0 mode can be calculated based on equations (1) and (2) respectively [25].

$$f_{A_0} = \frac{2\pi h}{\lambda^2}\sqrt{\frac{E}{12(1-\upsilon^2)\rho}}\frac{1}{\sqrt{\frac{\pi^2 h^2}{3\lambda^2}+1}} \tag{1}$$

$$f_{S_0} = \frac{1}{\lambda}\sqrt{\frac{E}{(1-\upsilon^2)\rho}} \tag{2}$$

where λ, E, υ, ρ and h are wavelength, Young's modulus, Poisson's ratio, density, and thickness of the device, which are listed in Table 1 [26]. The parameters of the composite ZnO/Al two layer structures were estimated depending on the material thickness ratio of ZnO and Al (1:10). For example, $E = (E_{ZnO}+10E_{Al})/11$. Frequency of the Rayleigh wave, f_R, can be calculated by: $f_R = v/\lambda$, in which v is the phase velocity for the sound wave, about 2600 m/s from literature of ZnO/Al foil substrate [17].

The calculated resonant frequencies of the A_0, S_0 and R_0 wave modes with different wavelengths are listed in Table 2. For the same wave mode the calculated resonant frequencies decrease as the

wavelength increases. Fig. 2a shows that the measured frequencies of A_0 mode for the devices with different wavelengths are identical to those calculated results.

The measured A_0 mode frequencies are slightly lower than those calculated data, which might be attributed to the thickness inhomogeneity and surface roughness of the ZnO films. Fig. 2b shows the frequency data of the S_0 and R_0 modes from measurement and calculation. Similarly to those of the A_0 mode, the measured frequencies of S_0 mode and R_0 mode are slightly lower than those of calculated results. The largest difference among the measured and calculated values is 6.66%.

Table 3 lists the wave velocities calculated based on the frequencies measured from different devices using the equation $v = \lambda \bullet f$. It can be seen that for A_0 mode, the wave velocity increases as the wavelength decreases. For A_0 mode of 800 μm devices, the wave velocity is as low as 685.6 m/s, whereas for A_0 mode of 64 μm devices, the wave velocities are as high as 4611 m/s, much higher than the R_0 mode. The wave velocities of S_0 or R_0 modes of the devices did not show significant changes as a function of the wavelength, as reported in Ref. [25, 26].

3.2. Characterization of flexibility of SAW devices

Flexibility, deformability and re-deformability of the Al foil based devices (64 μm, with a resonant frequency of 41.4 MHz) were characterized using a bending test rig. The foil substrate was subjected to different bending strains ε by putting steel tubes with different diameters under it ($\varepsilon = t/2r \times 100\%$, where t is the material thickness and r is the bending curve radius), and transmission signals (S21) were continuously measured during device bending. As shown in Fig. 3a, after bending the substrate to a large strain of 1.375% (when $\theta = 90°$), there was still transmission signal detected, however the signal amplitude became much weaker. When the

device was bent to flat state the transmission signal was also recovered. Fig. 3b shows the relationship among bending strength, resonant frequency and transmission signal amplitude. It can be seen that the resonant frequency and the S21 signal decrease as the bending strain increases. When the bending strain is larger than 1% to 1.2%, the resonant frequency and the amplitude decrease sharply.

To examine the bending fatigue/deformation reproducibility performance of the devices, a repeated bending test of the device with the wavelength of 128 μm at a strain of 0.6% was conducted for 2000 cycles by using a steel tube with appropriate size as a support. Fig. 4 shows the measured resonant frequency and amplitude of transmission signals (S21) for the device after different bending cycles. The frequency and amplitude decrease as the bending cycles are increased; however, they become relatively stable after 500 cycles. Optical observation of the surface morphology of the device after 500 and 2000 bending cycles showed that some cracks are formed on film surface, which can explain the reason for the variations of the frequency and amplitude. The possible reason could be due to generation of small cracks in the ZnO thin film during early bending cycles, which stops after 500 cycles. Another possible reason could be the slight deformation of Al foils during bending. However these cracks were largely isolated, and there were still propagation pathways after the bending. That's the reason we believe why the device can still work and the transmission signal can still be detected. Before the cyclic bending, the centre frequency and transmission loss of the device were 24.12 MHz and -44.99 dB, respectively, whereas those values were 23.9 MHz and -58.815 dB after 2000 bending cycles. Clearly, the device still shows good transmission signals after bending for thousands cycles, indicating a good fatigue resistance for a long term cycling applications.

3.3. SAW microfluidics tests

In order to demonstrate one of the potential applications of the flexible/deformable acoustofluidic device, microfluidic tests were performed by putting deionized waters with size of 2.5 μL on the surface of the propagation path of the SAW devices (here we selected devices with wavelengths of 64, 400 and 800 μm). Fig. 5 shows the movement of the droplet versus time for ZnO/Al SAW devices with different wavelengths. For the 64 μm wavelength device, with an input RF signal of 41.1 MHz and 3.8 Watts, there was significant internal streaming observed with a typical butterfly pattern. With the input power was increased to 9.2 Watts, capillary waves started to appear on the surface of the droplet. After maintaining the RF power for about 700 ms with RF power of 22.5 Watts, or about 100ms at 35 Watts, the droplets were pumped forward as shown in Fig. 5a. The last image in Fig. 5a also shows the local jetting of satellite liquid drops for the 64 μm SAW device during droplet movement, indicating the efficiency of the droplet agitation effect. For 400 μm device (Fig. 5b) with an input RF signal (13.17 MHz and 32 Watts) from the left side, the droplet was also pumped forward clearly using the S0 mode wave, in which jumping of droplet can be clearly seen. For the 800 μm device as shown in Fig. 5b, with an input RF signal (6.6 MHz and 32 Watts) from the left side, the droplet was also transported efficiently using the lamb wave (S0 mode) generated by the device.

The calculated velocities of the 2.5 μL droplets from the recorded videos for the ZnO/Al SAW devices with wavelengths of 800 μm, 400 μm, 100 μm and 64 μm are shown in Fig. 6. For the four devices we investigated, the velocity of the droplet movement increases significantly as the input RF power increases. With the same input RF power, the velocity of the droplet transportation is larger for the device with a smaller wavelength. Velocity data of the droplet movement for the 100 μm wavelength device are much larger than those of 800 μm wavelength

device at the same input power. This could be attributed to the large dissipation of vibration energy into the Al foil substrates at a larger wavelength of 800 μm. Results also showed that it is difficult to transport the droplet using the A_0 mode frequencies of the devices, but this will need further investigation. For the devices working at A_0 mode, the wave vibration amplitude seems much smaller than the S_0 mode (see Fig. 1 as an example), and the wave energy is less generated than that of S_0 mode. Consequently, the movement of the droplet would be easier to be observed for the device working at S_0 mode than A_0 mode.

3.4. Demonstration of flexibility in microfluidics

Flexible and deformable microfluidics has been demonstrated using the deformed ZnO/Al foil devices. Fig. 7a shows that the device (with wavelength of 400 μm) has been bent up to different height levels, where the positions of the IDTs (where RF signal applied) and the droplets are in different heights. After applying the RF signal with 13.05 MHz (S_0 mode) and power of 40 Watts, the droplet (2.5 μL) showed significant vibration and jumping.

The second demonstration (shown in Fig. 7b) is that the device (with wavelength of 400 μm) has been bent in the middle using a circular rod with a diameter of 4.7 mm. In this case, the IDTs and droplet are still in the same height, but the wave needs to propagate through a curved surface before reaching to the droplet (see Fig. 7b). After applying the RF signal with 2.917 MHz (A_0 mode) and an RF power of 22.5 Watts, significant vibration and moving of the droplet (2.5 μL) can be observed.

The third demonstration is that a SAW device was three-dimensionally twisted to a large angle of about 70 degrees as shown in Fig. 7c. With 6.6 MHz (S_0 mode) and 15 Watts RF signal input from left side, the vibration of the 2.5 μL droplet can be clearly observed. All the above results demonstrated the flexibility of the device and possibility for flexible sensing applications and long term cycling applications.

4. Conclusions

In summary, ZnO coated Al foil has been used to fabricate flexible and deformable devices for acoustofluidics. The wave frequency spectra and vibration modes of the ZnO/Al foil acoustic wave devices have been characterized and the results were in a good agreement with the results obtained from theoretical calculations. Flexibility and deformability of the ZnO/Al foil devices were demonstrated by the acoustic wave devices with bending strains up to 1.375%. Fatigue and cycling performance of the flexible devices have been tested by bending the devices with a fixed strain 0.6% for up to 2000 cycles, and the resonance frequency of the device decreased by 0.91%. Using the resonant frequencies from both the Lamb wave mode and Rayleigh wave mode, efficient acoustofluidic functions of streaming and pumping have been demonstrated. The flexibility of microfluidics from the ZnO/Al foil acoustic wave devices has been demonstrated.

Acknowledgements

The authors acknowledge Royal Academy of Engineering-Research Exchange with China and India, and the EPSRC (Engineering and Physical Sciences Research Council) Engineering Instrument Pool for providing the high speed video system (Photron XLR Express, VISION

Research Phantom MIRO 4, infrared video camera ThermaCAMTM SC640) , and NSFC under project No. 61274086.

References

[1] L. Zhou, A. Wanga, S-C. Wu, J. Sun, S. Park, and T. N. Jackson, Appl. Phys. Lett., 88, 083502 (2006).

[2] H. Jin, J. Zhou, X. He, W. Wang, H. Guo, S. Dong, D. Wang, Y. Xu, J. Geng, J.K. Luo and W.I. Milne, Sci. Rep., 3, 2140(2013).

[3] Y. Sun and J.A. Rogers, Adv. Mater., 19, 1897(2007).

[4] D-H. Kim, R. Ghaffari, N. Lu, and J.A. Rogers, Annu. Rev. Biomed. Eng., 14, 113(2012).

[5] D. Son, J. Lee, S. Qiao, R. Ghaffari, J. Kim, J.E. Lee, C. Song, S.J. Kim, D.J. Lee, S.W. Jun, S. Yang, M. Park, J. Shin, K. Do, M. Lee, K. Kang, C.S. Hwang, N. Lu, T. Hyeon, and D-H. Kim, Nat. Nanotech., 9, 397(2014).

[6] A. Nathan, A. Ahnood, M.T. Cole, S. Lee, Y. Suzuki, P. Hiralal, F. Bonaccorso, T. Hasan, L. Garcia-Gancedo, A. Dyadyusha, S. Haque, P. Andrew, S. Hofmann, J. Moultrie, D. Chu, A.J. Flewitt, A.C. Ferrari, M.J. Kelly, J. Robertson, G. Amaratunga, W.I. Milne, Proc. of IEEE, 100, 1486(2012).

[7] M. Focke, D. Kosse, C. Muller, H. Reinecke, R. Zengerle, and F. von Stetten, Lab Chip, 10, 1365(2010).

[8] X.S. Zhou, C. Zhao, R. Hou, J. Zhang, K.J. Kirk, D. Hutson, Y.J. Guo, P.A. Hu, S.M. Peng, X.T. Zu, and Y.Q. Fu, Ultrasonics, 54, 1991(2014).

[9] H.F. Pang, Y.Q. Fu, G.A. Zhang, R.Z. Hou, K. Kirk, D. Hudson, L.P. Wang, X.T. Zu, F. Placido, Ultrasonics, 53, 1264(2013).

[10] H.F. Pang, G.A. Zhang, Y.L. Tang, Y.Q.Fu, L.P. Wang, X.T. Zu, and F. Placido, Appl. Surf. Sci., 259, 747(2012).

[11] S. Shoaee, J. Briscoe, J.R. Durrant and S. Dunn, Adv. Mater., 26, 263(2014).

[12] S. Lee, S. Bae, L. Lin, Y. Yang, C. Park, S-W. Kim, S.N. Cha, H. Kim, Y.J. Park, and Z.L. Wang, Adv. Func. Mater., 23, 2445(2013).

[13] V. Rajendran, M. Koike, K.Y. Hashimoto, and M. Yamaguchi, Jap. J. Appl. Phys., 31, 216(1992)

[14] J. R. Friend and L. Y. Yeo, Rev. Mod. Phys., 83, 647(2011).

[15] A. Wixforth, J. Assoc. Lab. Automa., 11, 399(2006).

[16] L. Y. Yeo, J. R. Friend, Annu. Rev. Fluid Mech., 46, 379(2014).

[17] Y.Q. Fu, J.K. Luo, X.Y. Du, A.J. Flewitt, Y. Li, G.H. Markx, A.J. Walton, and W.I. Milne, Sensors and Actuators B: Chemical, 143, 606(2010).

[18] J.K. Luo, Y.Q. Fu, Y. Li, X.Y. Du, A.J. Flewitt, A.J. Walton, W.I. Milne, J. of Micromech. and Microeng. 19, 054001(2009).

[19] Y.Q. Fu, L. Garcia-Gancedo, H.F. Pang, S. Porro, Y.W. Gu, X. T. Zu, F. Placido, J.I.B. Wilson, A.J. Flewitt, W.I. Milne, Biomicrofluidics, 6, 013864 (2012).

[20] Y.Q. Fu, Y. Li, C. Zhao, F. Placido, and A.J. Walton, Appl. Phys. Lett., 101, 194101(2012).

[21] J. Zhou, M. DeMiguel-Ramos, L. Garcia-Gancedo, E. Iborra, J.Olivares, H. Jin, J.K. Luo, A. S. Elhady, S. R. Dong, D.M. Wang, Y.Q. Fu, Sens. Actuat. B, 202, 984(2014).

[22] J. Chen, X. He, W. Wang, W. Xuan, J. Zhou, X. Wang, S. R. Dong, S. Garner, P. Cimob and J. K. Luo, J. Mater. Chem. C, **2**, 9109(2014).

[23] A.R. Rezk, J.R. Friend and L.Y. Yeo, Lab Chip, 14, 1802(2014).

[24] X. L. He, D. J. Li, J. Zhou, W. B. Wang, W. P. Xuan, S. R. Dong, H. Jin, and J. K. Luo, J. Mater. Chem C 1 (2013) 6210-6215.

[25] M.W. Liu, J.H. Li, J. Ma and C.H. Wang, Journal of Semiconductors, 2011, **32**, 44006.

[26] Kovac G T. Micromachined transducers sourcebook. New York: McGraw-Hill Science, 1998.

Table 1 The material parameters used for the calculation.

Material	Thickness h	Young's modulus E	Poisson's ratio υ	Density ρ
ZnO	5 μm	120 GPa	0.446	5610 kg/m^3
Al	50 μm	69 GPa	0.33	2700 kg/m^3

Table 2 Calculated resonant frequencies for the devices with different wavelengths.

Wavelength	800 μm	400 μm	200 μm	128 μm	100 μm	64 μm
A_0	0.86 MHz	3.36 MHz	13.45 MHz	26.71 MHz	39.28 MHz	73.14 MHz
S_0	6.95 MHz	13.9 MHz	27.81 MHz	43.44 MHz	55.61 MHz	86.89 MHz
R_0	3.25 MHz	6.5 MHz	13 MHz	20.3 MHz	26 MHz	40.6 MHz

Table 3 Calculated wave velocities of different modes for devices with different wavelengths based on measured results.

Wavelength	800 μm	400 μm	200 μm	128 μm	100 μm	64 μm
A_0	685.6 m/s	1174 m/s	1852 m/s	3091 m/s	3975 m/s	4611 m/s
S_0	5420 m/s	5280 m/s	5078 m/s	5018 m/s	5499 m/s	5484 m/s
R_0	2384 m/s	2652 m/s		2425 m/s	2440 m/s	2636 m/s

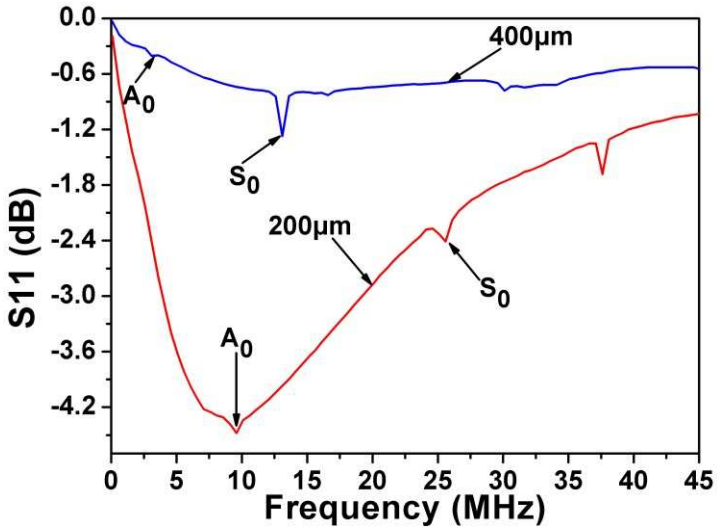

Fig. 1 Frequency response (S11) spectra of the Al foil SAW devices with different wavelengths (200 and 400 μm).

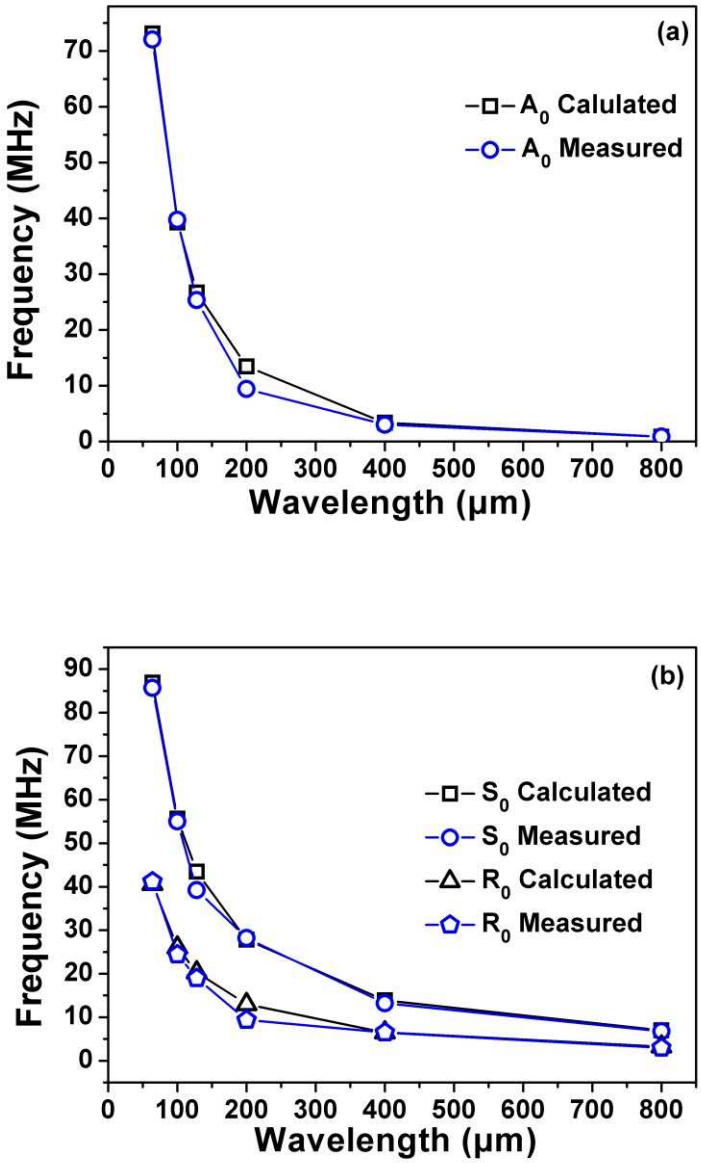

Fig. 2 Comparison of calculated and measured frequencies of A_0 modes (a); R_0 and S_0 modes (b) for the devices with different wavelengths.

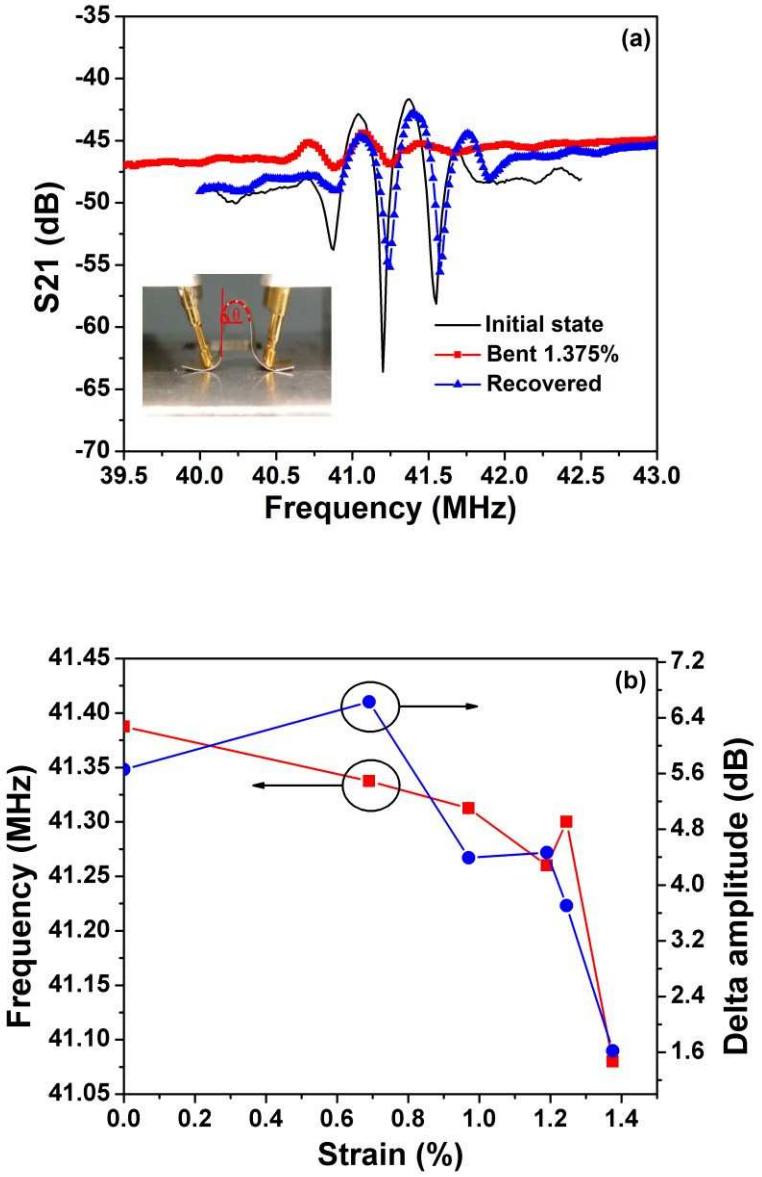

Fig. 3 (a) Comparison of transmission signals S12 of a device with bending strain of 0%, 1.375% and its return to flat shape; the embedded photo shows a side view of a bent Al foil SAW device at a maximum strain 1.375% when $\theta \cong 90°$; (b) The relationships among bending strain, amplitude peak height and frequency shift.

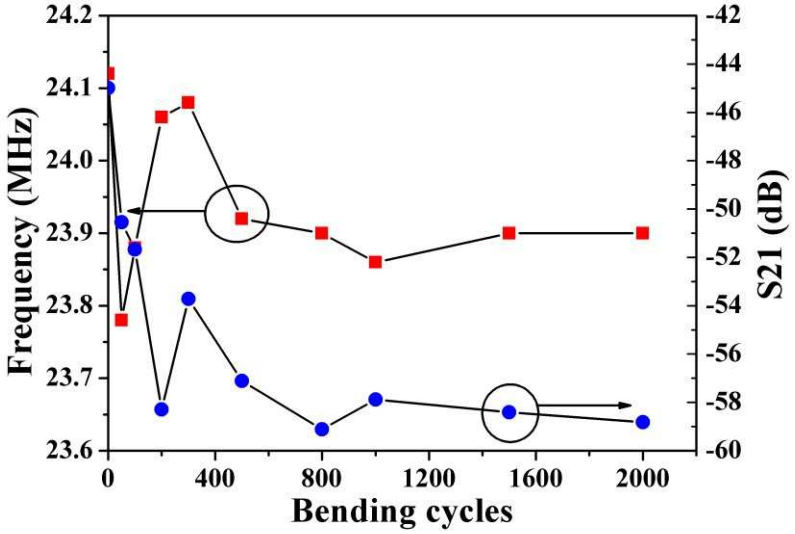

Fig. 4 Frequency and amplitude shift of the device with the wavelength of 128 μm after different bending cycles, with a bending strain of 0.6%.

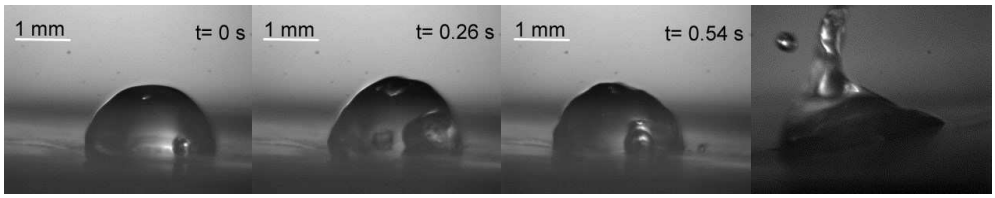

(a)

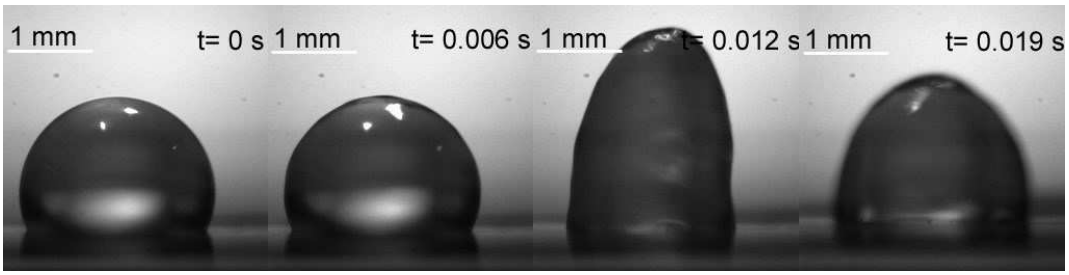

(b)

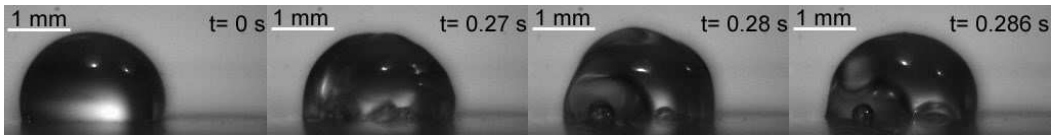

(c)

Fig. 5 Movements of the 2.5 μL droplets for: (a) R_0 mode (RF signal with 41.1 MHz and 35 Watts coming from right side) for 64 μm device; and (b) S_0 mode (RF signal with 13.17 MHz and 32 Watts coming from left side) for 400 μm device; and (c) S_0 mode (RF signal with 6.6 MHz and 32 Watts coming from left side) for 800 μm device.

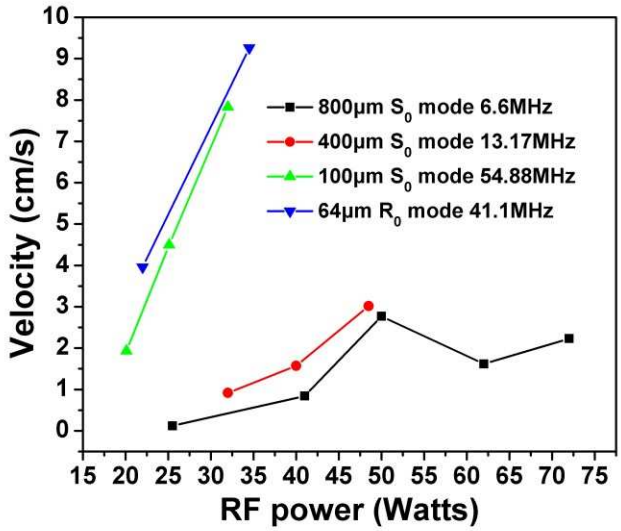

Fig. 6 Velocities of the droplet (2.5 uL) movement versus input power for devices with different wavelengths.

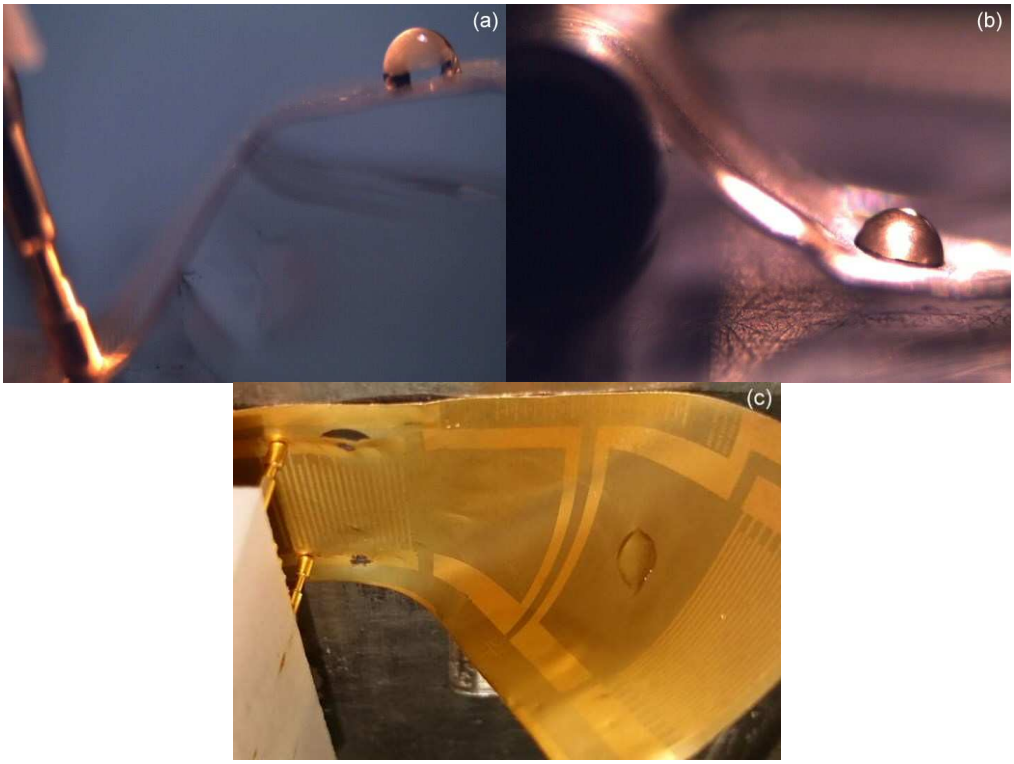

Fig. 7 Demonstration for flexibility of ZnO/Al SAW microfluidic devices.